Discrete Chirp-Fourier Transform and Its Application to Chirp Rate Estimation

Xiang-Gen Xia, *Senior Member, IEEE*

***Abstract*—The discrete Fourier transform (DFT) has found tremendous applications in almost all fields, mainly because it can be used to match the multiple frequencies of a stationary signal with multiple harmonics. In many applications, wideband and nonstationary signals, however, often occur. One of the typical examples of such signals is chirp-type signals that are usually encountered in radar signal processing, such as synthetic aperture radar (SAR) and inverse SAR imaging. Due to the motion of a target, the radar return signals are usually chirps, and their chirp rates include the information about the target, such as the location and the velocity.**

In this paper, we study discrete chirp-Fourier transform (DCFT), which is analogous to the DFT. Besides the multiple frequency matching similar to the DFT, the DCFT can be used to match the multiple chirp rates in a chirp-type signal with multiple chirp components. We show that when the signal length N is prime, the magnitudes of all the sidelobes of the DCFT of a quadratic chirp signal are 1, whereas the magnitude of the mainlobe of the DCFT is $\sqrt{N}$. With this result, an upper bound for the number of the detectable chirp components using the DCFT is provided in terms of signal length and signal and noise powers. We also show that the N-point DCFT performs optimally when N is a prime.

***Index Terms*—Chirp-Fourier transform, chirp rate estimation, chirps.**

I. Introduction

THE DISCRETE Fourier transform (DFT) has been applied in almost all fields. The main reason is because the DFT matches the frequencies in a signal of multiple harmonics. In other words, if a signal has only several harmonics, the DFT of this signal has and only has peaks at the frequencies of the signal harmonics, and the peak values correspond to the signal powers at the corresponding harmonic frequencies. Therefore, the DFT can be used to estimate the Fourier spectrum of a signal, which is known as *spectrum estimation*, that plays an important role in digital signal processing applications. However, in order to have the DFT work well, a signal has to be stationary. Although the stationarity assumption applies in many applications, nonstationary signals often occur in some real applications. Examples of nonstationary signals are chirp-type signals that are encountered in radar signal processing, such as in synthetic aperture radar (SAR) and inverse SAR (ISAR) imaging; see, for example, [1]. In SAR imaging, when targets are moving, the radar return signals are chirps, in particular *quadratic chirps*, when the velocities of the moving targets are constant. In ISAR imaging, when targets have maneuvering motions, the radar return signals are also chirps. It is well known in the SAR and ISAR literature that the direct DFT applications to the radar return signals will smear the SAR or ISAR images of the targets. Furthermore, the chirp rates in the radar return signals include the important information about the moving targets, such as the velocities and the location parameters of the moving targets in SAR imaging. Therefore, the estimation of the chirp rates are critically important in these applications.

For chirp-type signals, besides frequencies of multiple harmonics, there are chirp rates of multiple chirps, and the DFT can be used only to match the multiple frequencies, but the multiple chirps, in this case, may even reduce the resolution of the frequency matching. The question of interest in this paper is to generalize the DFT and its properties to *discrete chirp-Fourier transform* (DCFT) and corresponding properties, which is used not only to match the multiple frequencies but to match the multiple chirp rates, simultaneously as well.

It should be noticed that there has been much research on chirp-type signals and their chirp rate estimations, such as high-order ambiguity functions [2]–[4], adaptive chirplet transforms [10], [11], and other polynomial phase signal estimations [7]–[9]. In addition, the chirp z-transform was proposed in [12] for the efficient DFT implementation but not for chirp rate estimation. However, the goal of this paper is for chirp signal analysis and is, therefore, different. We first generalize the DFT to the DCFT and then study the properties of the DCFT analogous to the DFT. In particular, we show that when signal length N is a *prime*, the magnitudes of all the sidelobes (i.e., when the chirp rate is not matched) of the DCFT of a single quadratic chirp signal without noise are 1, whereas the magnitude of the mainlobe (i.e., when the chirp rate and the harmonic frequency are both matched) of the DCFT is $\sqrt{N}$. The mainlobe and sidelobe magnitude ratio in this case is $\sqrt{N}$, which is shown to be optimal for a given length N. In other words, the DCFT performs optimally in the matching of the constant frequency and the chirp rate when the signal length N is a prime. When the chirp rate is precisely matched, the DCFT is reduced to the DFT. Notice that for any signal length N, the magnitudes of all the sidelobes of the DFT of a single harmonic signal without noise are 0, whereas the magnitude of the mainlobe of the DFT is $\sqrt{N}$. The mainlobe and sidelobe magnitude ratio in this case is infinity, which tells

Manuscript received May 12, 1999; revised July 16, 2000. This work was supported in part by the Office of Naval Research Young Investigator Program under Grant N00014-98-1-0644, the Air Force Office of Scientific Research (AFOSR) under Grant F49620-00-1-0086, and the National Science Foundation (NSF) CAREER under Grant MIP-9703377. The associate editor coordinating the review of this paper and approving it for publication was Prof. Gregori Vazquez.

The author is with Department of Electrical and Computer Engineering, University of Delaware, Newark, DE 19716 USA (e-mail: xxia@ee.udel.edu).

Publisher Item Identifier S 1053-587X(00)09308-9.

us that N many different harmonics can be estimated using the DFT when there is no noise. In general, unlike the DFT for the harmonic estimation, less than $\sqrt{N}$ many different chirps can be estimated using the DCFT. This paper is focused on quadratic chirps that are common in radar applications.

This paper is organized as follows. In Section II, we introduce the DCFT and study its basic properties for single component chirp signals. In Section III, we study the properties of the DCFT for multiple component chirp signals. We present an upper bound for the number of the components such that they are detectable using the DCFT. In Section IV, we study its connection with the analog chirp-Fourier transform. In Section V, we present some numerical examples.

II. Discrete Chirp-Fourier Transform and Its Basic Properties for Single Component Chirp Signals

Before going to the DCFT, let us first briefly recall the DFT. For a signal $x(n)$ with length N, its N-point DFT is defined as

$$X(k) = \frac{1}{\sqrt{N}} \sum_{n=0}^{N-1} x(n) W_N^{nk}, \qquad 0 \le k \le N-1 \quad (2.1)$$

where $W_N = \exp(-2\pi j/N)$. The key properties of the DFT are based on the following elementary identity

$$\sum_{n=0}^{N-1} W_N^{nk} = N\delta(k), \qquad 0 \le k \le N-1 \quad (2.2)$$

where $\delta(k)$ takes 1 when $k = 0$ and 0 otherwise. The identity (2.2) implies that if $x(n)$ is a single harmonic, i.e.,

$$x(n) = \exp\left(j2\pi \frac{k_0}{N} n\right)$$

for some integer k_0 with $0 \le k_0 \le N-1$, then its DFT matches the frequency k_0 perfectly, i.e.,

$$X(k) = \sqrt{N}\delta(k - k_0). \quad (2.3)$$

Based on this property, when $x(n)$ has I harmonics with $I \le N$, i.e.,

$$x(n) = \sum_{i=1}^{I} A_{k_i} \exp\left(j2\pi \frac{k_i}{N} n\right)$$

where $k_{i_1} \ne k_{i_2}$ for $i_1 \ne i_2$, its DFT matches these frequencies perfectly, i.e.,

$$X(k) = \sqrt{N} \sum_{i=1}^{I} A_{k_i} \delta(k - k_i) \quad (2.4)$$

where the peaks in the DFT domain are shown at all k_i, and the corresponding peak values are A_{k_i} for $i = 1, 2, \cdots, I$.

We now introduce the *discrete chirp-Fourier transform* (DCFT). Let $x(n)$, $0 \le n \le N-1$ be a signal of length N. Its N-point DCFT is defined as

$$X_c(k,l) = \frac{1}{\sqrt{N}} \sum_{n=0}^{N-1} x(n) W_N^{ln^2+kn}, \qquad 0 \le k, l \le N-1 \quad (2.5)$$

where k represents the constant frequencies and l represent the chirp rates. From the above DCFT, one can see that for each fixed l, $\{X_c(k,l)\}_{0\le k\le N-1}$ is the DFT of the signal $x(n)W_N^{ln^2}$. When $l = 0$, the DCFT is the same as the DFT. Therefore, the inverse DCFT (IDCFT) is

$$x(n) = W_N^{-ln^2} \frac{1}{\sqrt{N}} \sum_{k=0}^{N-1} X_c(k,l) W_N^{-kn}$$
$$0 \le n \le N-1 \quad (2.6)$$

where l is an arbitrarily fixed integer. The above connection between the DCFT and the DFT also suggests a fast algorithm to compute the DCFT, i.e., for each l, the FFT may be used to compute $X_c(k,l)$, $0 \le k \le N-1$. The computational complexity with this approach is, thus, $O(N^2 \log(N))$.

As a remark, the above chirp-Fourier transform is related to the fractional Fourier transform (FRFT), where the rotation angle is related to the variable l in the DCFT. For more about FRFT, see, for example, [13]–[17].

The above DCFT definition is not surprising to see by following the DFT definition. What is more interesting is its properties. Can it be used to match the chirp rates and the constant frequencies simultaneously? If so, how many of the chirp components can be matched simultaneously? Similar to the previous DFT study, let us first consider a single chirp signal

$$x(n) = W_N^{-(l_0 n^2 + k_0 n)} \quad (2.7)$$

where k_0 and l_0 are two integers with $0 \le k_0, l_0 \le N-1$. When k and l in the DCFT (2.5) precisely match the above k_0 and l_0, we have

$$X_c(k_0, l_0) = \sqrt{N}$$

which is called the *mainlobe* of the DCFT $X_c(k,l)$. The question of interest here is what happens when the chirp rate l and the constant frequency k do not match l_0 and k_0, i.e., what the *sidelobes* of the DCFT are. Is there a similar property for the DCFT as (2.3) for the DFT? To study these questions, we first have the following lemma.

Lemma 1: When N is a prime, we have the following identity: For $0 \le l, k \le N-1$

$$\left| \sum_{n=0}^{N-1} W_N^{ln^2+kn} \right| = \begin{cases} N, & l = 0 \text{ and } k = 0 \\ \sqrt{N}, & l \ne 0 \\ 0, & l = 0 \text{ but } k \ne 0. \end{cases} \quad (2.8)$$

Proof: Let

$$P(k,l) \triangleq \sum_{n=0}^{N-1} W_N^{ln^2+kn}.$$

Then, for $0 < l \le N-1$

$$\begin{aligned}|P(k,l)|^2 &= \sum_{n=0}^{N-1} W_N^{ln^2+kn} \sum_{m=0}^{N-1} W_N^{-lm^2-km} \\ &= \sum_{n=0}^{N-1}\sum_{m=0}^{N-1} W_N^{(n-m)\,(l(n+m)+k)} \\ &\triangleq \sum_{n=0}^{N-1}\sum_{e=0}^{N-1} W_N^{e(l(2n-e)+k)} \\ &= \sum_{e=0}^{N-1}\left(\sum_{n=0}^{N-1} W_N^{2eln}\right) W_N^{-e^2l+ek} \qquad (2.9)\end{aligned}$$

where $e = n-m$, and the new range of e in the summation in Step 1 is from the periodicity of W_N^{ln} in terms of the integer variable n for any integer l. When N is a prime, $2el$ for $0 < l \le N-1$, and $0 \le e \le N-1$ is a multiple of N if and only if e is a multiple of N, i.e., $e = 0$. Thus

$$\sum_{n=0}^{N-1} W_N^{2eln} = 0 \quad \text{for } 0 < e, l \le N-1.$$

Therefore, $|P(k,l)|^2 = N$ when $l \neq 0$. When $l = 0$, $P(k,l)$ is reduced to (2.2). This proves the lemma. **q.e.d.**

From the second half of the above proof, one can see why N needs to be prime in order for the second equality in (2.8) to hold. From this lemma, we immediately have the following result.

Theorem 1: Let $x(n)$ be a single chirp

$$x(n) = W_N^{-(l_0n^2+k_0n)} \qquad (2.10)$$

for some integers k_0 and l_0 with $0 \le k_0, l_0 \le N-1$. If the length N is a prime, then its DCFT magnitude has the following form:

$$|X_c(k,l)| = \begin{cases} \sqrt{N}, & \text{when } l = l_0 \text{ and } k = k_0 \\ 1, & \text{when } l \neq l_0 \\ 0, & \text{when } l = l_0 \text{ but } k \neq k_0. \end{cases} \qquad (2.11)$$

This result tells us that for a single quadratic chirp, the peak or the mainlobe of its DCFT has value $\sqrt{N}$ and appears at (k_0, l_0) in the DCFT domain and that the sidelobes are not above 1. In other words, the DCFT of a single quadratic chirp matches its chirp rate l_0 and its constant frequency k_0 simultaneously. Surprisingly, one can see that all the magnitudes of the sidelobes, unless the chirp rate is matched, are all the same, which is 1.

In chirp rate and constant frequency estimation, the smaller the sidelobe magnitudes of the DCFT, the better the performance of the estimation. When N is a prime, from (2.11), the maximal sidelobe magnitude of the DCFT is 1, i.e.,

$$\max_{(k,l)\neq(k_0,l_0)} |X_c(k,l)| = 1, \quad \text{when } N \text{ is a prime.} \qquad (2.12)$$

One might want to ask what will happen when N is not a prime. The following result tells us that the maximal sidelobe magnitude is the minimal when N is a prime, i.e., the N-point DCFT performs the best when N is a prime in the estimation of chirp rates and constant frequencies. This will be also seen from the numerical simulations in Section V.

Theorem 2: Let $x(n)$ be the same as in Theorem 1, i.e., have the form in (2.10). If the length N is not a prime, then the maximal sidelobe magnitude of the DCFT satisfies

$$\max_{(k,l)\neq(k_0,l_0)} |X_c(k,l)| \ge \sqrt{2}. \qquad (2.13)$$

Proof: To prove (2.13), it is enough to prove that when N is not a prime, the following inequality holds:

$$\max_{(k,l)\neq(0,0)} |P(k,l)|^2 \ge 2N \qquad (2.14)$$

where $P(k,l)$ is defined in the Proof of Lemma 1. Assume N is not a prime, and let $N = N_1N_2$ with $N_1 \ge 2$ and $N_2 \ge 2$.

Case i): Both N_1 and N_2 are odd. In this case, let $l = N_1$ and $k = 0$. Then, by (2.9)

$$\begin{aligned}|P(k,l)|^2 &= \sum_{e=0}^{N-1}\left(\sum_{n=0}^{N-1} W_{N_2}^{2en}\right) W_{N_2}^{-e^2} \\ &= N_1 \sum_{e=0}^{N-1}\left(\sum_{n=0}^{N_2-1} W_{N_2}^{2en}\right) W_{N_2}^{-e^2}.\end{aligned}$$

Since N_2 is odd, $2e$ is a multiple of N_2 if and only if e is a multiple of N_2. Thus

$$\sum_{n=0}^{N_2-1} W_{N_2}^{2en} = 0, \quad \text{if } e \text{ is not a multiple of } N_2.$$

Therefore, by setting $e = e_1N_2$, we have

$$\begin{aligned}|P(k,l)|^2 &= N_1 \sum_{e_1=0}^{N_1-1}\left(\sum_{n=0}^{N_2-1} W_{N_2}^{2e_1N_2n}\right) W_{N_2}^{-e_1^2N_2^2} \\ &= N_1 \sum_{e_1=0}^{N_1-1} N_2 = N_1^2N_2 \ge 2N.\end{aligned}$$

Case ii): One of N_1 and N_2 is even. Without loss of generality, we may assume $N_2 = 2$. Let $k = l = N_1$. In this case, $W_N^{2eln} = 1$. Thus, by (2.9)

$$|P(k,l)|^2 = N \sum_{e=0}^{N-1} W_2^{-e(e-1)}.$$

Notice that $e(e-1)$ is always even, which implies $W_2^{-e(e-1)} = 1$. Therefore

$$|P(k,l)|^2 = N^2 \geq 2N.$$

By combining Cases i) and ii), (2.14) is proved. **q.e.d.**

By this result, in what follows, we only consider prime N. The above results are based on the assumption that both l_0 and k_0 in (2.10) are integers. In practice, these two parameters may not be precisely integers. Next, we want to briefly discuss the DCFT performance when they are not integers but are close to integers. The reason why we only consider the case when l_0 and k_0 are close to integers is because of the following argument.

Let us consider an analog chirp signal

$$x_a(t) = \exp(j(\beta_0 t^2 + \alpha_0 t)) \tag{2.15}$$

and consider the sampling $t = n/N^{1/3}$. Then, the sampled chirp becomes

$$\begin{aligned}\tilde{x}(n) &\triangleq x_a\left(\frac{n}{N^{1/3}}\right) = \exp\left(j\left(\frac{\beta_0}{N^{2/3}}n^2 + \frac{\alpha_0}{N^{1/3}}n\right)\right) \\ &= W_N^{-(\tilde{l}_0 n^2 + \tilde{k}_0 n)}\end{aligned} \tag{2.16}$$

where $\tilde{l}_0 = \beta_0 N^{-1/3}/(2\pi)$ and $\tilde{k}_0 = \alpha_0 N^{-2/3}/(2\pi)$. Therefore, when N is large enough (i.e., the sampling rate is fast enough), there exist integers l_0 and k_0 such that

$$\tilde{l}_0 = \frac{\beta_0 N^{-1/3}}{2\pi} \approx l_0 \quad \text{and} \quad \tilde{k}_0 = \frac{\alpha_0 N^{-2/3}}{2\pi} \approx k_0. \tag{2.17}$$

This implies that the real chirp rate is $\beta_0 \approx 2\pi l_0 N^{1/3}$ and that the real constant frequency is $\alpha_0 \approx 2\pi k_0 N^{2/3}$ when integers l_0 and k_0 are estimated. It also tells us that for a practical chirp signal $x_a(t)$ in (2.15), we only need to consider the discrete chirp signal $\tilde{x}(n)$ in (2.16) with parameters $\tilde{l}_0$ and $\tilde{k}_0$ close to integers.

We now consider a discrete chirp signal

$$\tilde{x}(n) = W_N^{-(\tilde{l}_0 n^2 + \tilde{k}_0 n)} \tag{2.18}$$

where

$$|\tilde{l}_0 - l_0| < \epsilon \quad \text{and} \quad |\tilde{k}_0 - k_0| < \eta \tag{2.19}$$

where l_0 and k_0 are two integers with $0 \leq l_0, k_0 \leq N-1$, and ϵ, and η are two positive numbers. By using the Taylor expansion of $\exp(jy)$ in terms of jy, it is not hard to see that

$$|\exp(jy) - 1| \leq |y|\exp(|y|), \qquad y \in \mathbf{R}. \tag{2.20}$$

Thus, for $0 \leq n \leq N-1$

$$\begin{aligned}|\tilde{x}(n) - x(n)| &\leq \frac{\epsilon n^2 + \eta n}{N}\exp(\epsilon n^2 + \eta n) \\ &< (\epsilon N + \eta)\exp(\epsilon N + \eta) \triangleq \xi\end{aligned} \tag{2.21}$$

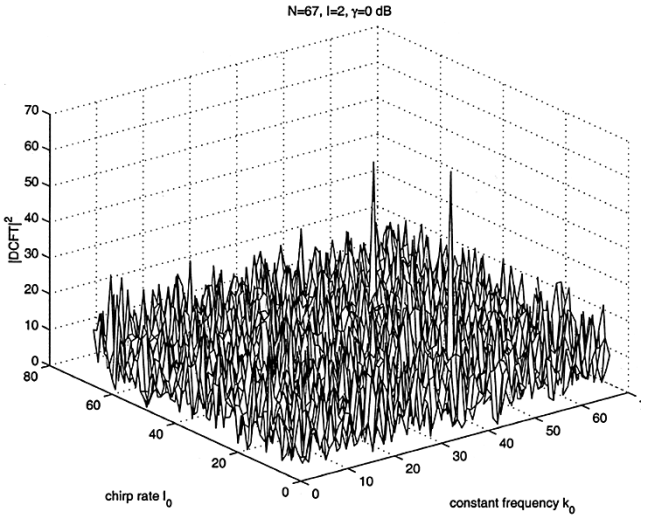

(a)

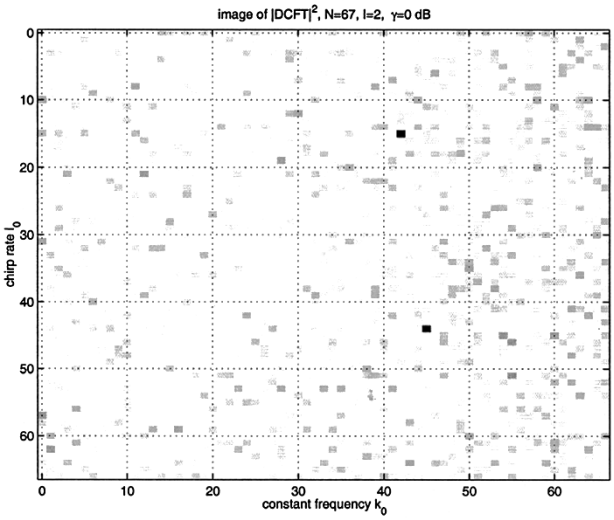

(b)

Fig. 1. DCFT of two chirp components with additive SNR $\gamma = 0$ dB. (a) Three-dimensional plot. (b) Image.

where $x(n) = W_N^{-(l_0 n^2 + k_0 n)}$, which is the same as in (2.10). By using Theorem 1 and (2.21), the following result is therefore proved.

Theorem 3: Let $\tilde{x}(n)$ satisfy (2.18) and (2.19), and let $\tilde{X}_c(k,l)$ be its DCFT. Then

$$|\tilde{X}_c(k,l)| \begin{cases} > \sqrt{N}(1-\xi), & \text{if } l = l_0 \text{ and } k = k_0 \\ < 1 + \sqrt{N}\xi, & \text{if } l \neq l_0 \\ < \sqrt{N}\xi, & \text{if } l = l_0 \text{ and } k \neq k_0 \end{cases} \tag{2.22}$$

where ξ is defined in (2.21).

From this theorem, one can see that as long as the chirp rate error level ϵ and the constant frequency error level η are low enough (i.e., $\tilde{l}_0$ and $\tilde{k}_0$ are close enough to integers l_0 and k_0, i.e., $\epsilon, \eta \approx 0$, which can be achieved when the sampling rate is fast enough), the DCFT of the chirp signal still has the peak property as in Theorem 1. We will see some numerical examples in Section V.

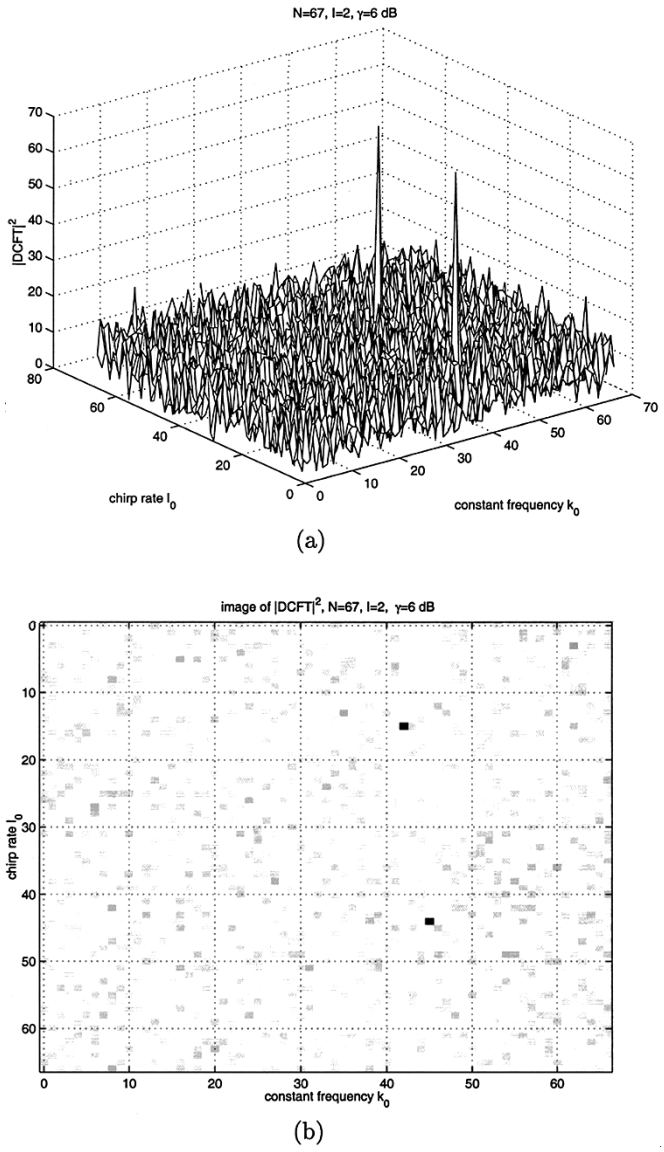

Fig. 2. DCFT of two chirp components with additive SNR $\gamma = 6$ dB. (a) Three-dimensional plot. (b) Image.

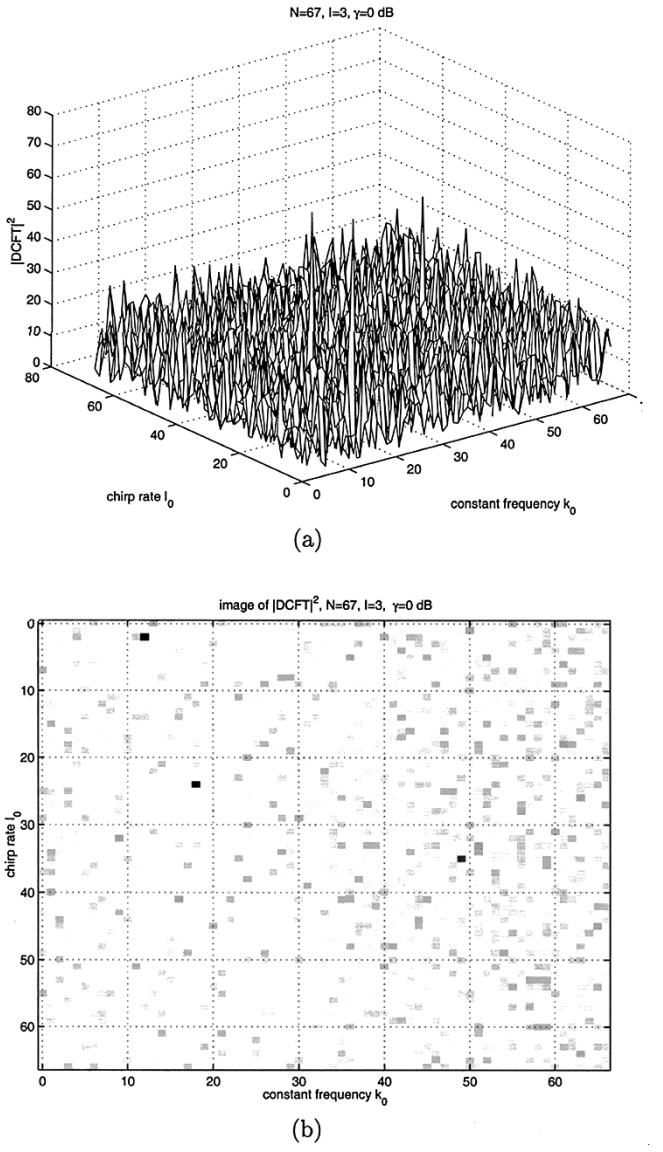

Fig. 3. DCFT of three chirp components with additive SNR $\gamma = 0$ dB. (a) Three-dimensional plot. (b) Image.

III. DCFT Properties for Multiple Component Chirp Signals

We next consider a multiple component chirp signal $x(n)$ of the form

$$x(n) = \sum_{i=1}^{I} A_i W_N^{-(l_i n^2 + k_i n)} + z(n) \tag{3.1}$$

where $z(n)$ is an additive i.i.d. noise with mean 0 and variance σ^2, $|A_i|^2 > 0$ is the signal power of the ith chirp component, and $(k_{i_1}, l_{i_1}) \neq (k_{i_2}, l_{i_2})$ for $i_1 \neq i_2$. For $i = 1, 2, \cdots, I$, let

$$x_i(n) = A_i W_N^{-(l_i n^2 + k_i n)}. \tag{3.2}$$

Then, the DCFT $X_c(k,l)$ of $x(n)$ is

$$X_c(k,l) = \sum_{i=1}^{I} X_c^{(i)}(k,l) + Z_c(k,l)$$

where $X_c^{(i)}(k,l)$ is the DCFT of the ith chirp component $x_i(n)$, and $Z_c(k,l)$ is the DCFT of noise $z(n)$. From the study in Section II, we know that each $X_c^{(i)}(k,l)$ has a peak at (k_i, l_i) with peak value $|A_i|\sqrt{N}$, and the maximal off peak value is $|A_i|$. What we are interested in here is whether there is a peak of $X_c(k,l)$ at each (k_i, l_i), $1 \leq i \leq I$. If there is a peak at (k_i, l_i), then a chirp component with constant frequency k_i and chirp rate l_i is detected. To study this question, let us calculate the mean magnitude of $X_c(k,l)$. We first calculate the mean $|X_c(k,l)|$ at (k_i, l_i). For $i = 1, 2, \cdots, I$

$$\begin{aligned} E|X_c(k_i,l_i)| &\geq |X_c^{(i)}(k_i,l_i)| - \sum_{\tau \neq i} |X_c^{(\tau)}(k_i,l_i)| - E|Z_c(k_i,l_i)| \\ &\overset{1}{\geq} |A_i|\sqrt{N} - \sum_{\tau \neq i} |A_\tau| - (E|Z_c(k_i,l_i)|^2)^{1/2} \end{aligned} \tag{3.3}$$

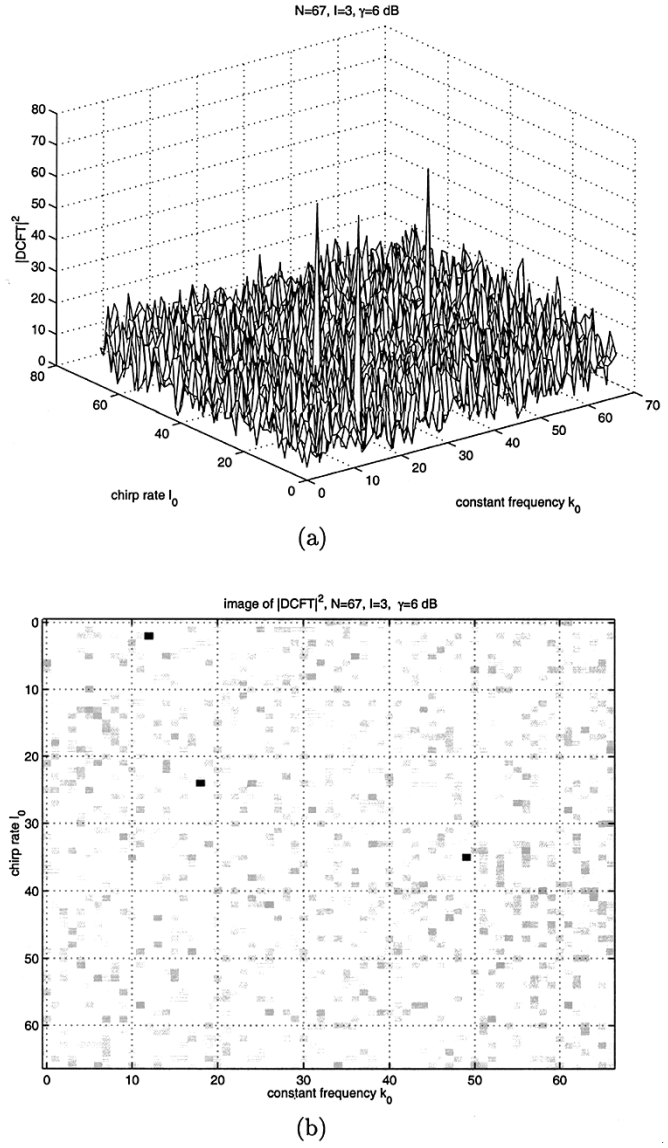

Fig. 4. DCFT of three chirp components with additive SNR $\gamma = 6$ dB. (a) Three-dimensional plot. (b) Image.

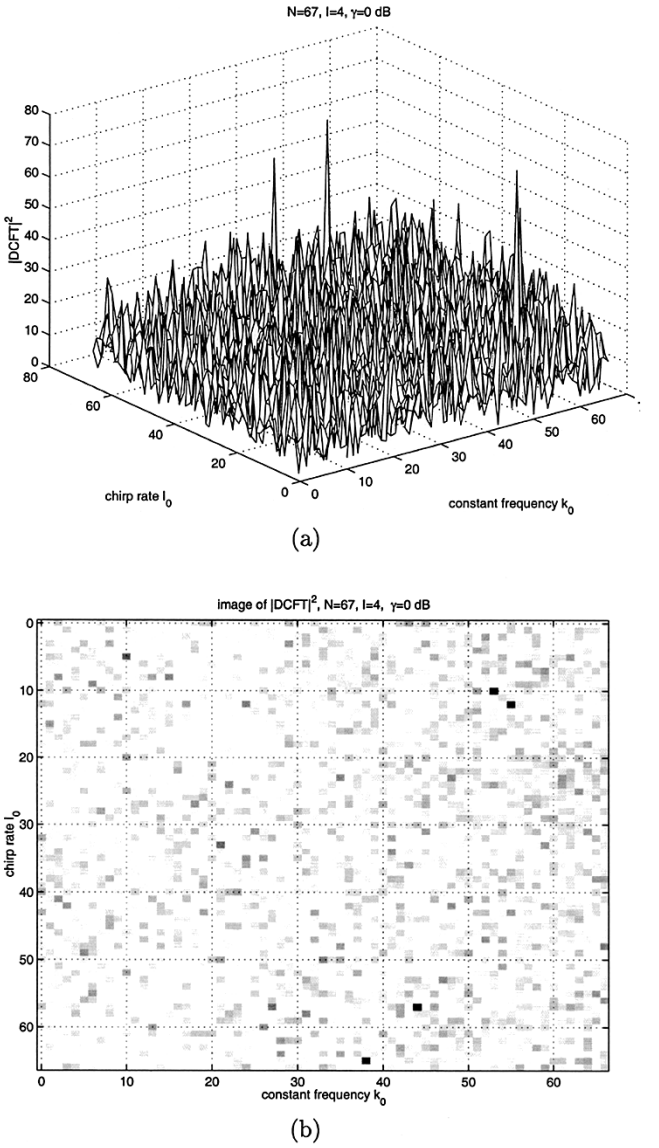

Fig. 5. DCFT of four chirp components with additive SNR $\gamma = 0$ dB. (a) Three-dimensional plot. (b) Image.

where the inequality in Step 1 is because $E|Z_c(k_i,l_i)| \le (E|Z_c(k_i,l_i)|^2)^{1/2}$ from the Schwarz inequality with respect to the expectation E. Thus, to estimate the lower bound of the mean magnitude $|X_c(k_i,l_i)|$, we need to estimate the mean power of the DCFT of the noise $z(n)$. Since for any fixed l, $Z_c(k,l)$ is the DFT of $z(n)W_N^{ln^2}$, the energy of $Z_c(k,l)$ in terms of the frequency variable k is the same as the one of $z(n)W_N^{ln^2}$, i.e., the one of $z(n)$. This proves

$$E|Z_c(k,l)|^2 = \sigma^2. \tag{3.4}$$

Therefore, for $i = 1, 2, \cdots, I$ by (3.3) and (3.4), we have

$$E|X_c(k_i,l_i)| \ge \sqrt{N}|A_i| - \sum_{\tau \ne i} |A_\tau| - \sigma. \tag{3.5}$$

Furthermore, for $(k,l) \ne (k_i,l_i)$ for $i = 1, 2, \cdots, I$

$$\begin{aligned} E|X_c(k,l)| &\le \sum_{i=1}^{I} |X_c^{(i)}(k,l)| + (E|Z_c(k,l)|^2)^{1/2} \\ &\le \sum_{i=1}^{I} |A_i| + \sigma. \end{aligned} \tag{3.6}$$

By comparing (3.5) and (3.6), there are peaks at (k_i,l_i) in the DCFT domain if

$$\sqrt{N}|A_i| - \sum_{\tau \ne i} |A_\tau| - \sigma > \sum_{i=1}^{I} |A_i| + \sigma$$

or

$$|A_i| > \frac{2}{\sqrt{N}-1} \left(\sum_{\tau \ne i} |A_\tau| + \sigma \right). \tag{3.7}$$

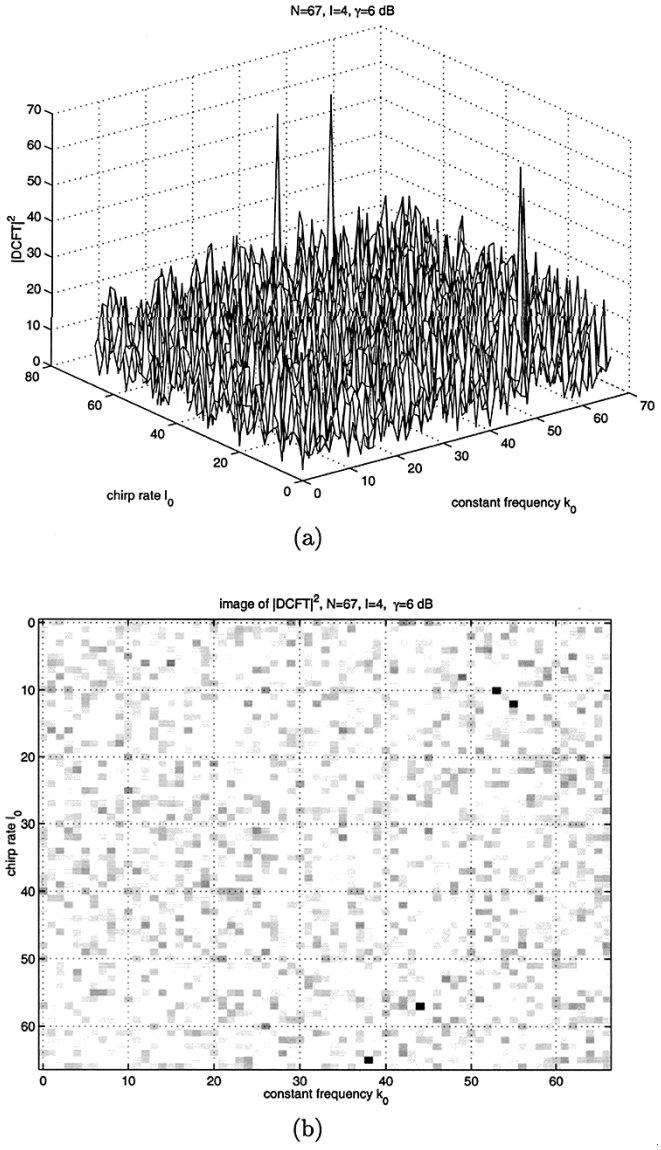

Fig. 6. DCFT of four chirp components with additive SNR $\gamma = 6$ dB. (a) Three-dimensional plot. (b) Image.

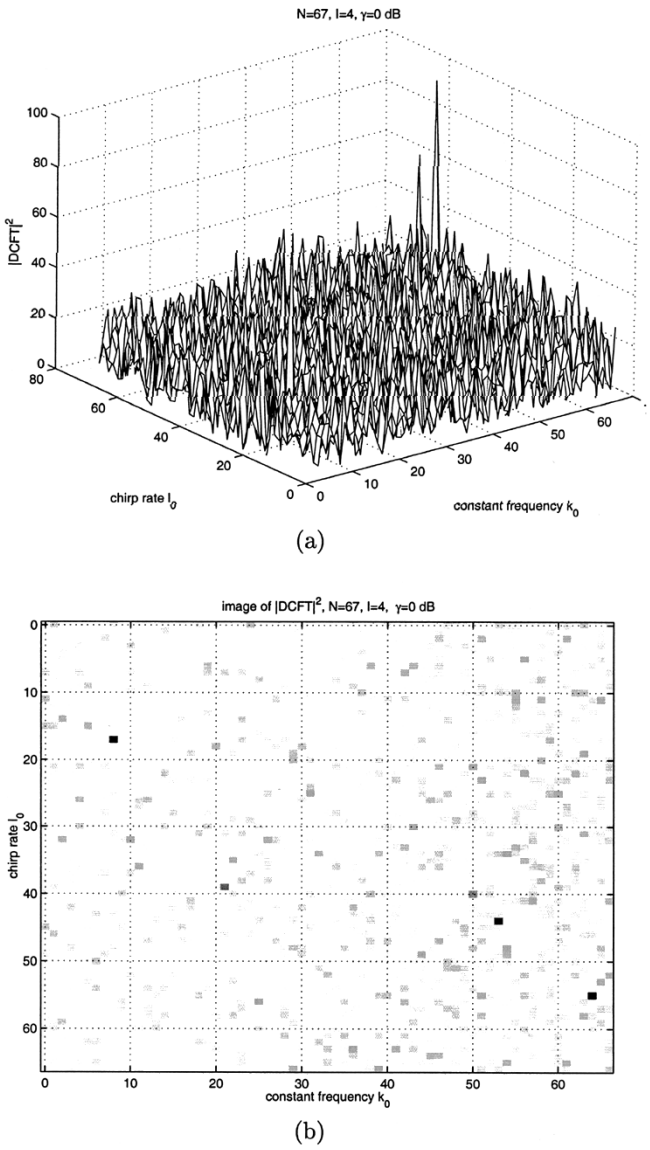

Fig. 7. DCFT of another set of four chirp components with additive SNR $\gamma = 0$ dB. (a) Three-dimensional plot. (b) Image.

Theorem 4: Consider a multiple component chirp signal $x(n)$ in (3.1) with components at different constant frequency and chirp rate pairs (k_i, l_i) of power $|A_i|^2$ for $i = 1, 2, \cdots, I$. Its DCFT magnitudes at (k_i, l_i) are lower bounded by

$$E|X_c(k_i, l_i)| \geq \sqrt{N}|A_i| - \sum_{\tau \neq i} |A_\tau| - \sigma \qquad i = 1, 2, \cdots, I \tag{3.8}$$

and its DCFT magnitudes at other (k, l) are upper bounded by

$$E|X_c(k, l)| \leq \sum_{i=1}^{I} |A_i| + \sigma, \quad (k, l) \neq (k_i, l_i) \qquad i = 1, 2, \cdots, I. \tag{3.9}$$

For each i with $1 \leq i \leq I$, a peak in the DCFT domain appears at (k_i, l_i) if the inequality (3.7) holds.

From (3.7), one can see that when the number I of multiple chirp components is fixed, all the peaks at (k_i, l_i) for $i = 1, 2, \cdots, I$ will appear in the DCFT domain as long as the signal length N—a prime—is sufficiently large. In other words, when the signal is sufficiently long, all the chirp components can be detected by using the DCFT.

We next consider the special case when all the signal powers $|A_i|^2$ of the different chirp components are the same, i.e.

$$|A_i| = A, \quad \text{for } i = 1, 2, \cdots, I.$$

In this case, (3.7) becomes

$$1 > \frac{2}{\sqrt{N} - 1} \left(I - 1 + \frac{\sigma}{A} \right) = \frac{2}{\sqrt{N} - 1} \left(I - 1 + \frac{1}{\sqrt{\gamma}} \right)$$

where γ is the signal-to-noise ratio (SNR)

$$\gamma = \frac{A^2}{\sigma^2}. \tag{3.10}$$

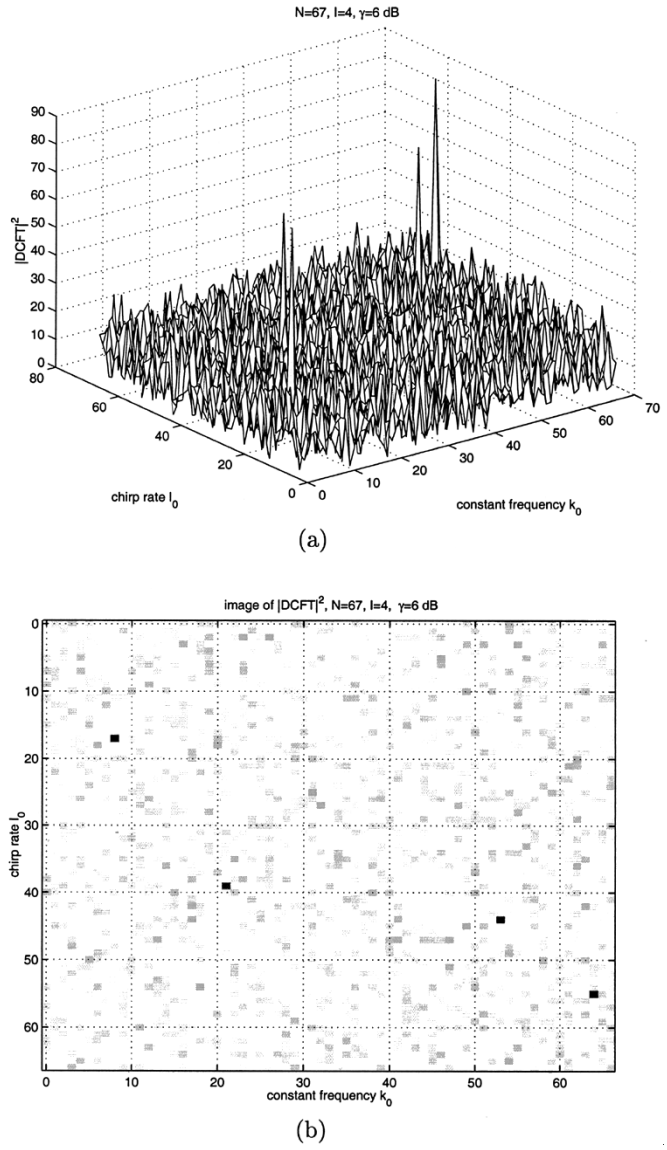

Fig. 8. DCFT of another set of four chirp components with additive SNR γ = 6 dB. (a) Three-dimensional plot. (b) Image.

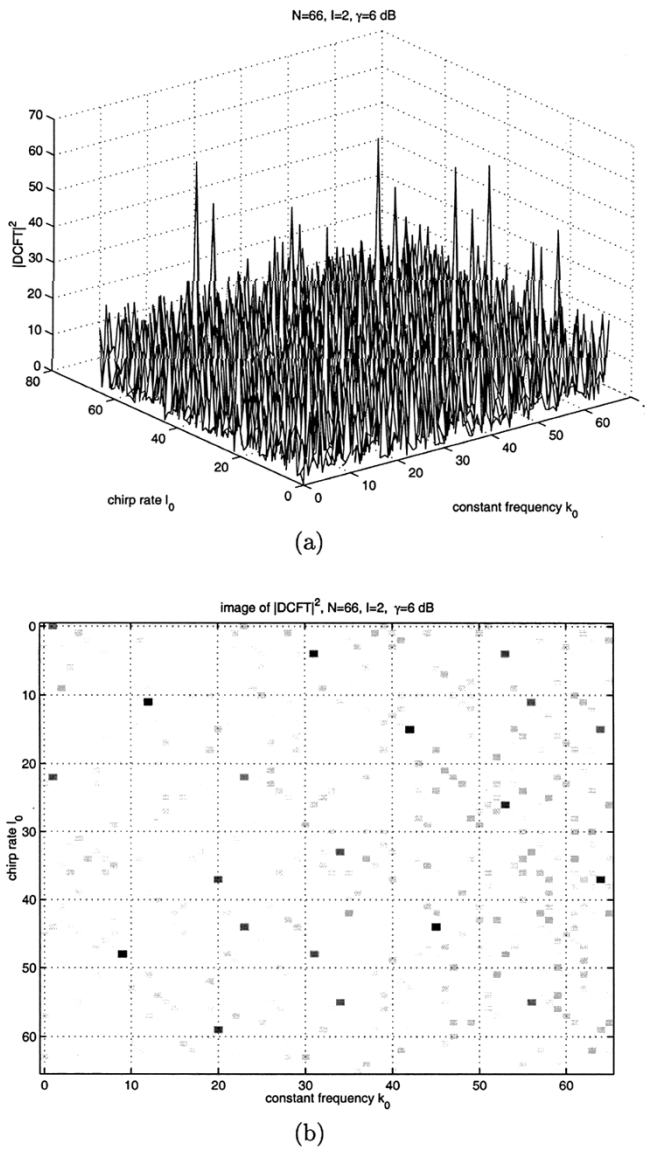

Fig. 9. DCFT of two chirp components with additive SNR γ = 6 dB and signal length N+ 66. (a) Three-dimensional plot. (b) Image.

In other words, given the SNR γ, all peaks at (k_i, l_i) for $i = 1, 2, \cdots, I$ appear in the DCFT domain if the number of chirp components satisfies

$$I < \frac{\sqrt{N}+1}{2} - \frac{1}{\sqrt{\gamma}}. \tag{3.11}$$

This gives us the following corollary.

Corollary 1: Let $x(n)$ be of the form (3.1) with all equal powers $|A_i|^2 = A^2$ and the SNR γ defined in (3.10). Then, there are peaks at (k_i, l_i) for $i = 1, 2, \cdots, I$ if the number I of the chirp components satisfies the upper bound (3.11).

The above corollary basically says that in the case when all signal powers of the multiple chirp components are the same, the chirp components can be detected using the DCFT if the number of them is less than $\sqrt{N}/2$ when the signal length N is sufficiently large. From the simulation results in Section V, one will see that the upper bound in (3.11) is already optimal, i.e., tight.

Similar to the single chirp DCFT performance analysis in Theorem 3, when the chirp rate and the constant frequency parameters l_i and k_i are not integers, the above results for multiple chirp DCFT can be generalized. Some numerical examples will be presented in Section V.

IV. Connection to the Analog Chirp-Fourier Transform

In this section, we want to see the relationship of the DCFT and the analog chirp-Fourier transform (ACFT). Let us first see the ACFT. For an analog signal $x_a(t)$, its ACFT is

$$X_{c,a}(\alpha, \beta) = \int_{-\infty}^{\infty} x_a(t) \exp(-j(\beta t^2 + \alpha t))\, dt \tag{4.1}$$

where α and β are real. When $x_a(t)$ is a quadratic chirp, i.e.,

$$x_a(t) = \exp(j(\beta_0 t^2 + \alpha_0 t)) \tag{4.2}$$

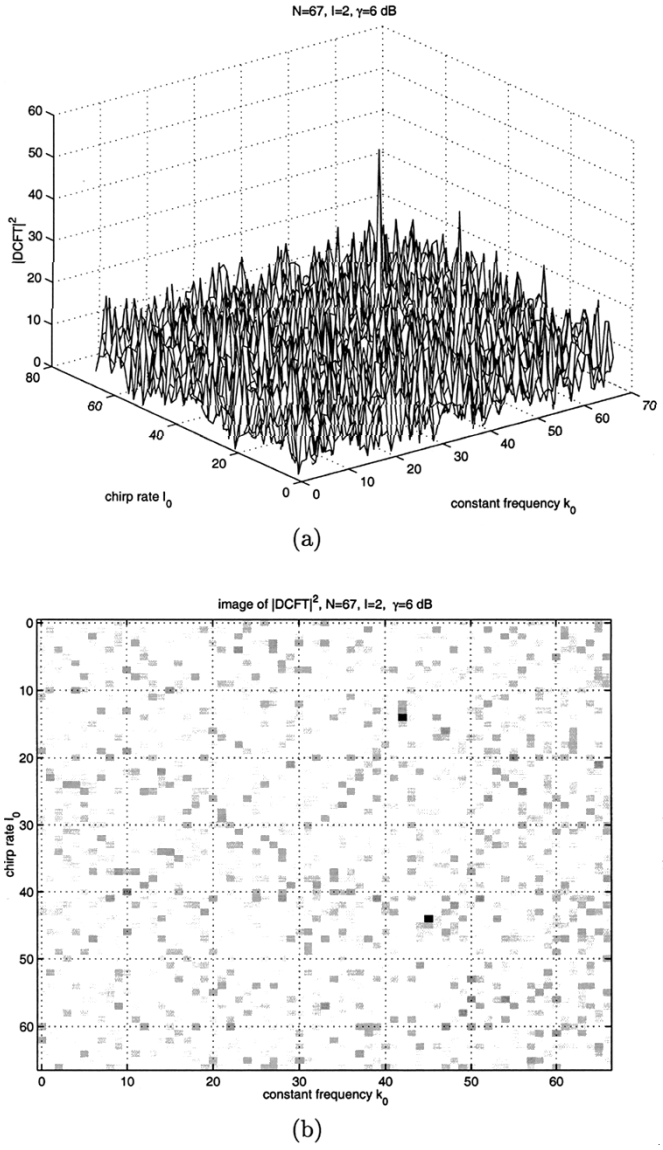

Fig. 10. DCFT of two chirp components (41.9897, 15.0180), (45.0037, 43.9968) with additive SNR $\gamma = 6$ dB. (a) Three-dimensional plot. (b) Image.

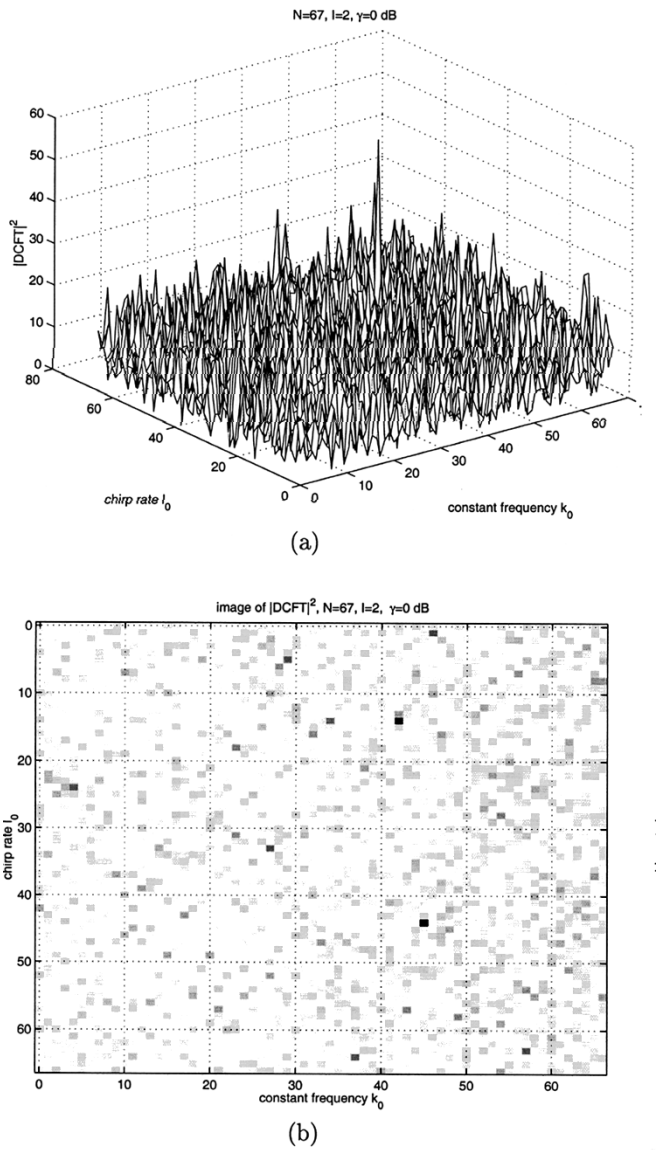

Fig. 11. DCFT of two chirp components (41.9897, 15.0180), (45.0037, 43.9968) with additive SNR $\gamma = 0$ dB. (a) Three-dimensional plot. (b) Image.

the ACFT is

$$\begin{aligned} X_{c,a}(\alpha,\beta) &= \int_{-\infty}^{\infty} \exp(j[(\beta_0-\beta)t^2 + (\alpha_0-\alpha)t])\, dt \\ &= 2\int_0^{\infty} \cos(\beta_0-\beta)t^2 \cos(\alpha_0-\alpha)t\, dt \\ &\quad + 2j\int_0^{\infty} \sin(\beta_0-\beta)t^2 \cos(\alpha_0-\alpha)t\, dt \\ &= \frac{1}{|\beta_0-\beta|^{1/2}}\,(1+\operatorname{sign}(\beta_0-\beta)) \\ &\quad \cdot \exp\left(-j\,\frac{(\alpha_0-\alpha)^2}{4(\beta_0-\beta)}\right) \end{aligned} \tag{4.3}$$

where (4.3) is from [18]. Clearly, when the constant frequency α_0 and the chirp rate β_0 are both matched, i.e., when $\alpha = \alpha_0$ and $\beta = \beta_0$, the ACFT $X_{c,a}(\alpha,\beta) = \infty$, and otherwise, $X_{c,a}(\alpha,\beta)$ is a finite value, i.e., $X_{c,a}(\alpha,\beta) < \infty$ for $\beta \neq \beta_0$ or $\alpha \neq \alpha_0$.

To consider the connection with the DCFT, let us consider the following samplings for the above analog parameters t, α, and β:

$$t := \frac{n}{N^{1/3}}, \quad \beta := \frac{2\pi n}{N^{1/3}}, \quad \alpha := \frac{2\pi n}{N^{2/3}} \tag{4.4}$$

where N is a positive integer. The reason for this sampling method is for getting the DCFT form studied in the previous sections, and the difference of the samplings between the chirp rate β and the constant frequency α is due to the power difference between the chirp term t^2 and the constant frequency term t. Truncate $x_a(t)$ such that it is zero for $t \notin [0, N^{2/3}]$. Sample $x_a(t)$ into $x(n) = x_a(n/N^{1/3})$ for $n = 0, 1, 2, \cdots, N-1$. In this case, the integral in (4.1) can be discretized

$$\begin{aligned} X_{c,a}\left(\frac{k}{N^{2/3}}, \frac{l}{N^{1/3}}\right) &\approx \frac{1}{N^{1/3}} \sum_{n=0}^{N-1} x(n) W_N^{ln^2+kn} \\ &= \frac{N^{1/2}}{N^{1/3}}\, X_c(k,l). \end{aligned}$$

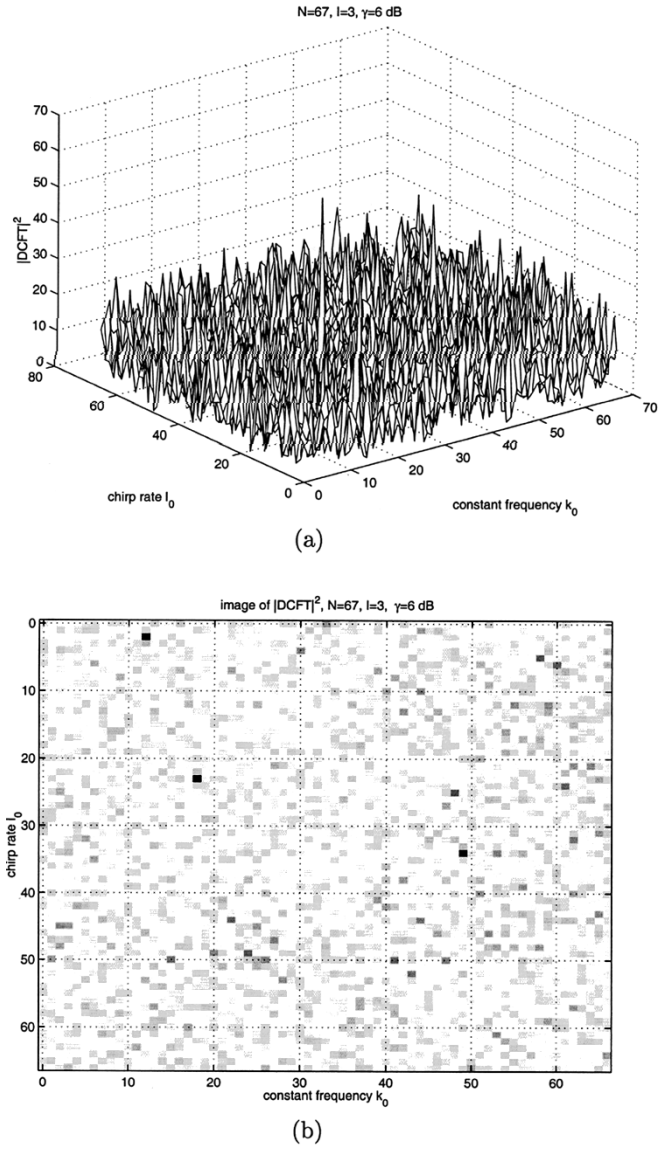

Fig. 12. DCFT of three chirp components (12.0050, 1.9883), (48.9875, 35.0063), (17.9825, 24.0004) with additive SNR $\gamma = 6$ dB. (a) Three-dimensional plot. (b) Image.

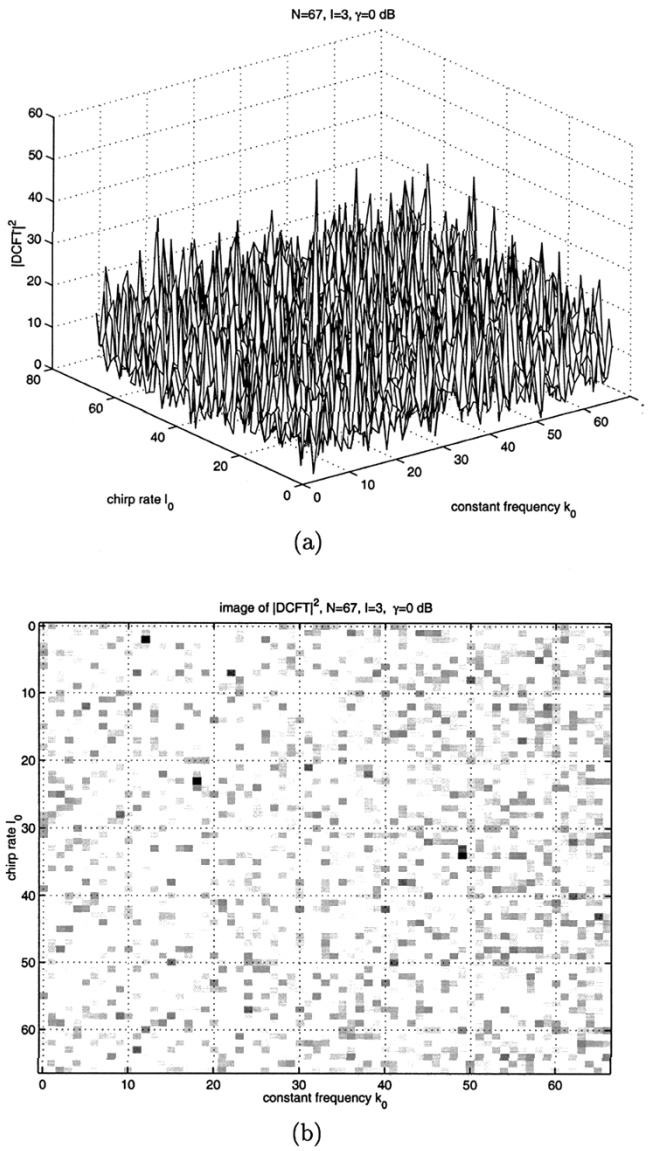

Fig. 13. DCFT of two chirp components (12.0050, 1.9883), (48.9875, 35.0063), (17.9825, 24.0004) with additive SNR $\gamma = 0$ dB. (a) Three-dimensional plot. (b) Image.

In other words

$$X_c(k,l) \approx N^{-1/6} X_{c,a}\left(\frac{k}{N^{2/3}}, \frac{l}{N^{1/3}}\right) \tag{4.5}$$

which gives a connection between the DCFT and the ACFT.

V. Numerical Simulations

In this section, we want to see some simple numerical simulations. Two signal lengths are considered: $N = 67$ and $N = 66$. We first see some examples when $N = 67$. Two different SNRs γ in (3.10) are considered, which are $\gamma_1 = 1$ (0 dB) and $\gamma_2 = 4$ (6 dB). For the first SNR γ_1, the upper bound in (3.11) for the number I of the detectable chirp components is 3, i.e., $I \le I_1 = 3$. For the second SNR γ_2, the upper bound in (3.11) for the number I of the detectable chirp components is 4, i.e., $I \le I_2 = 4$. In the following, three different numbers $I = 2, 3, 4$ of chirp components are simulated, where the constant frequencies k_i and the chirp rates l_i for $i = 1, 2, \cdots, I$ are arbitrarily chosen. The corresponding amplitudes A_i are set to be all 1.

Figs. 1 and 2 show the DCFT's of signals with two chirp components at $(k_i, l_i) = (42,15)$, (45, 44) and the SNR's $\gamma = \gamma_1 = 0$ dB and $\gamma = \gamma_2 = 6$ dB in (3.10), respectively. Figs. 3 and 4 show the DCFT's of signals with three chirp components at $(k_i, l_i) = (12, 2)$, (49, 35), (18, 24), and the SNR's $\gamma = \gamma_1 = 0$ dB and $\gamma = \gamma_2 = 6$ dB in (3.10), respectively. Figs. 5 and 6 show the DCFT's of signals with four chirp components at $(k_i, l_i) = (44, 57)$, (38, 65), (53, 10), (55, 12) and the SNR's $\gamma = \gamma_1 = 0$ dB and $\gamma = \gamma_2 = 6$ dB in (3.10), respectively. One can see from Fig. 5 that although the upper bound for I is 3 when the SNR $\gamma = \gamma_1 = 0$ dB, the four peaks can be seen in the DCFT domain. This is, however, not always true from the following examples. Figs. 7 and 8 show the DCFT's of another set of two signals with four chirp components at $(k_i, l_i) = (64,$

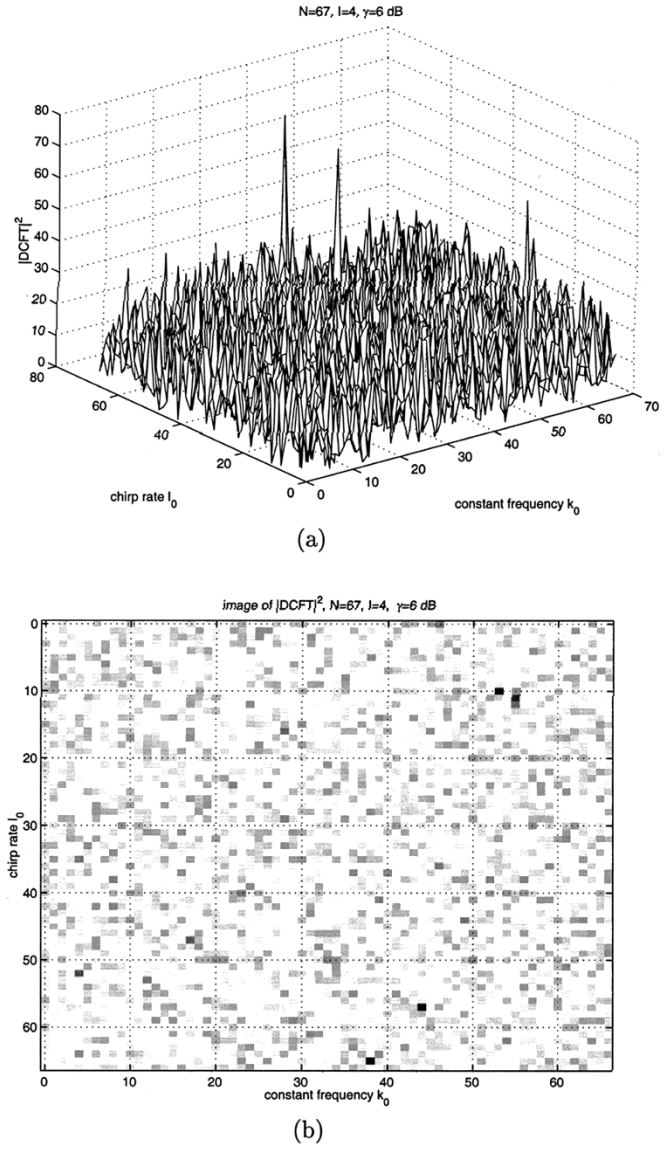

Fig. 14. DCFT of four chirp components (43.9977, 56.9989), (38.0013, 64.9920), (52.9976, 9.9991), (54.9898, 12.0094) with additive SNR $\gamma = 6$ dB. (a) Three-dimensional plot. (b) Image.

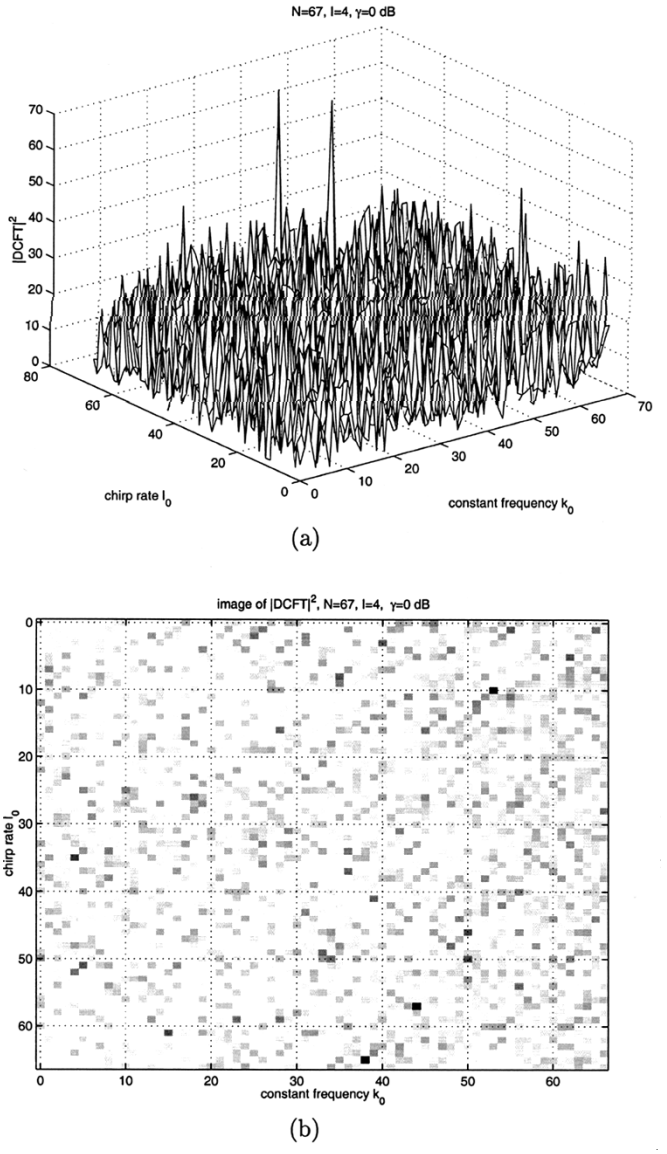

Fig. 15. DCFT of two chirp components (43.9977, 56.9989), (38.0013, 64.9920), (52.9976, 9.9991), (54.9898, 12.0094) with additive SNR $\gamma = 0$ dB. (a) Three-dimensional plot. (b) Image.

55), (21, 39), (8, 17), (53, 44), and the SNR's $\gamma = \gamma_1 = 0$ dB and $\gamma = \gamma_2 = 6$ dB in (3.10), respectively. One can see from Fig. 7 that the four peaks ($I = 4$) are not clear, which is because the upper bound for I in (3.11) is 3 when $\gamma = \gamma_1 = 0$ dB. The four peaks in Fig. 8 are, however, clear because the upper bound for I in (3.11) is 4 when $\gamma = \gamma_2 = 6$ dB.

When $N = 66$, we consider the two chirp components $(k_i, l_i) = (42, 15), (45, 44)$ in Fig. 2 with the SNR $\gamma = \gamma_2 = 6$ dB. Its DCFT is shown in Fig. 9. Clearly, it fails to show the two peaks, which illustrates the difference of the DCFT with respect to having prime and nonprime length.

We next want to see some examples when the chirp rate and the constant frequency parameters l_i and k_i are not but close to integers, i.e., $\epsilon, \eta \approx 0$. The parameter errors are randomly added with Gaussian distributions. Figs. 10 and 11 show the DCFT's of the two chirp components (k_i, l_i) = (41.9897, 15.0180), (45.0037, 43.9968) that are distorted from the chirp components in Figs. 1 and 2. Figs. 12 and 13 show the DCFT's of the three chirp components $(k_i, l_i) = (12.0050, 1.9883)$, (48.9875, 35.0063), (17.9825, 24.0004) that are distorted from the chirp components in Figs. 3 and 4. Figs. 14 and 15 show the DCFT's of the four chirp components $(k_i, l_i) =$ (43.9977, 56.9989), (38.0013, 64.9920), (52.9976, 9.9991), (54.9898, 12.0094) that are distorted from the chirp components in Figs. 5 and 6. One can see that unlike in Figs. 5 and 6, in Figs. 14 and 15, the four peaks are not all shown well, which is due to the additional distortions of the integer chirp rate and constant frequency parameters l_i and k_i, as we have studied in Theorem 3.

VI. Conclusion

In this paper, we studied the discrete chirp-Fourier transform (DCFT) for discrete quadratic chirp signals. The approach is analogous to the one of the DFT. We showed that when the signal length N is prime, all the sidelobes (i.e., when the chirp

rates or the constant frequencies are not matched) of the DCFT are not above 1, whereas the mainlobe (i.e., when the chirp rates and the constant frequencies are matched simultaneously) of the DCFT is $\sqrt{N}$. We showed that this is optimal, i.e., when N is not a prime, the maximal sidelobe magnitude of the DCFT is greater than 1 (in fact, we showed that the maximal sidelobe magnitude of the DCFT is greater than $\sqrt{2}$). We also presented an upper bound in terms of signal length N and SNR for the number of the detectable chirp components using the DCFT. Simulations were presented to illustrate the theory. A connection of the DCFT with the analog chirp-Fourier transform was also presented.

Although the DCFT was defined for quadratic chirps that are quite common in radar applications, it is not hard to generalize to higher order chirps. Notice that the DCFT for higher order chirps may not have the precise values but some roughly low values of the sidelobes obtained in Section s II and III for quadratic chirps. However, it might be possible but more tedious to calculate the values of the sidelobes of the DCFT for higher order chirps when the higher order powers of $P(k,l)$ in (2.9) in the Proof of Lemma 1 is used. Another comment we would like to make here is that similar to the spectrum estimation, when the chirp rate and the constant frequency are not integers, other high resolution techniques may exist and are certainly interesting.

ACKNOWLEDGMENT

The author would like to thank the reviewers for their constructive comments, in particular, for their suggestions of adding the analysis of the DCFT when the chirp parameters (k_i, l_i) are not all integers, which improves the clarity of the manuscript.

REFERENCES

[1] D. R. Wehner, *High-Resolution Radar*, 2nd ed. Norwell, MA: Artech House, 1995.
[2] S. Peleg and B. Porat, "Estimation and classification of signals with polynomial phase," *IEEE Trans. Inform. Theory*, vol. 37, pp. 422–430, 1991.
[3] B. Porat, *Digital Processing of Random Signals, Theory and Methods*. Englewood Cliffs, NJ: Prentice-Hall, 1994.
[4] S. Peleg and B. Friedlander, "The discrete polynomial-phase transform," *IEEE Trans. Signal Processing*, vol. 43, pp. 1901–1914, Aug. 1995.
[5] T. J. Abatzoglou, "Fast maximum likelihood joint estimation of frequency and frequency rate," *IEEE Trans. Aerosp. Electron. Syst.*, vol. AES-22, pp. 708–715, Nov. 1986.
[6] S. Peleg and B. Porat, "The Cramer-Rao lower bound for signals with constant amplitude and polynomial phase," *IEEE Trans. Signal Processing*, vol. 39, pp. 749–752, Mar. 1991.
[7] R. Kumaresan and S. Verma, "On estimating the parameters of chirp signals using rank reduction techniques," in *Proc. 21st Asilomar Conf. Signals, Syst., Comput.*, Pacific Grove, CA, 1987, pp. 555–558.
[8] P. M. Djuric and S. M. Kay, "Parameter estimation of chirp signals," *IEEE Trans. Acoust., Speech, Signal Processing*, vol. 38, pp. 2118–2126, Dec. 1990.
[9] M. Z. Ikram, K. Abed-Meraim, and Y. Hua, "Estimating the parameters of chirp signals: An iterative approach," *IEEE Trans. Signal Processing*, vol. 46, pp. 3436–3441, Dec. 1998.
[10] S. Qian, D. Chen, and Q. Yin, "Adaptive chirplet based signal approximation," in *Proc. ICASSP*, Seattle, WA, 1998.
[11] G. Wang and Z. Bao, "ISAR imaging of maneuvering targets based on chirplet decomposition," , to be published.
[12] L. R. Rabiner, R. W. Schafer, and C. M. Rader, "The chirp z-transform algorithm and its applications," *Bell Syst. Tech. J.*, vol. 48, pp. 1249–1292, May–June 1969.
[13] V. Namias, "The fractional order Fourier transform and its application to quantum mechanics," *J. Inst. Math. Appl.*, vol. 25, pp. 241–265, 1980.
[14] A. C. McBride and F. H. Kerr, "On Namias' fractional Fourier transforms," *IMA J. Appl. Math.*, vol. 39, pp. 150–175, 1987.
[15] L. B. Almeida, "The fractional Fourier transform and time-frequency representations," *IEEE Trans. Signal Processing*, vol. 42, pp. 3084–3091, Nov. 1994.
[16] A. W. Lohmann, "Image rotation, Wigner rotation and the fractional Fourier transform," *J. Opt. Soc. Amer. A*, vol. 10, pp. 2181–2186, 1993.
[17] D. Mendlovic and H. M. Ozaktas, "Fractional Fourier transformations and their optical implementation: I," *J. Opt. Soc. Amer. A*, vol. 10, pp. 1875–1881, 1993.
[18] I. N. Bronshtein and K. A. Semendyayev, *Handbook of Mathematics*. New York: Van Nostrand Reinhold, 1985.

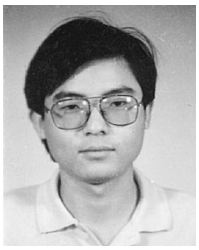

Xiang-Gen Xia (M'97–SM'00) received the B.S. degree in mathematics from Nanjing Normal University, Nanjing, China, the M.S. degree in mathematics from Nankai University, Tianjin, China, and the Ph.D. degree in electrical engineering from the University of Southern California (USC), Los Angeles, in 1983, 1986, and 1992, respectively.

He was a Lecturer at Nankai University from 1986 to 1988, a Teaching Assistant at the University of Cincinnati, Cincinnati, OH, from 1988 to 1990, a Research Assistant at USC from 1990 to 1992, and a Research Scientist at the Air Force Institute of Technology from 1993 to 1994. He was a Senior/Research Staff Member at Hughes Research Laboratories, Malibu, CA, from 1995 to 1996. In September 1996, he joined the Department of Electrical and Computer Engineering, University of Delaware, Newark, DE, where he is currently an Associate Professor. His current research interests include communication systems including equalization and coding; SAR and ISAR imaging of moving targets, wavelet transform, and multirate filterbank theory and applications; time–frequency analysis and synthesis; and numerical analysis and inverse problems in signal/image processing. He is the author of *Modulated Coding for Intersymbol Interference Channels* (New York: Marcel Dekker, 2000).

Dr. Xia received the National Science Foundation (NSF) Faculty Early Career Development (CAREER) Program Award in 1997 and the Office of Naval Research (ONR) Young Investigator Award in 1998. He is currently an Associate Editor of the IEEE TRANSACTIONS ON SIGNAL PROCESSING and a Member of the Signal Processing for Communications Technical Committee of the IEEE Signal Processing Society.